PNAS

Supporting Information for

Crosstalk between Paneth and tuft cells drives dysbiosis and inflammation in the gut mucosa

Nathalie Coutry[1,#,*], Julie Nguyen[1,#], Salima Soualhi[1,#], François Gerbe[1], Victoria Meslier[3], Valérie Dardalhon[2], Mathieu Almeida[3], Benoit Quinquis[3], Florence Thirion[3], Fabien Herbert[1], Imène Gasmi[1], Ali Lamrani[1], Alicia Giordano[1], Pierre Cesses[1], Laure Garnier[1], Steeve Thirard[1], Denis Greuet[1], Chantal Cazevieille[4], Florence Bernex[5], Christelle Bressuire[3,9], Douglas Winton[6], Ichiro Matsumoto[7], Hervé M. Blottière[3,8], Naomi Taylor[2] and Philippe Jay[1,*]

[*] Corresponding authors: philippe.jay@igf.cnrs.fr, Nathalie.coutry@igf.cnrs.fr

This PDF file includes:

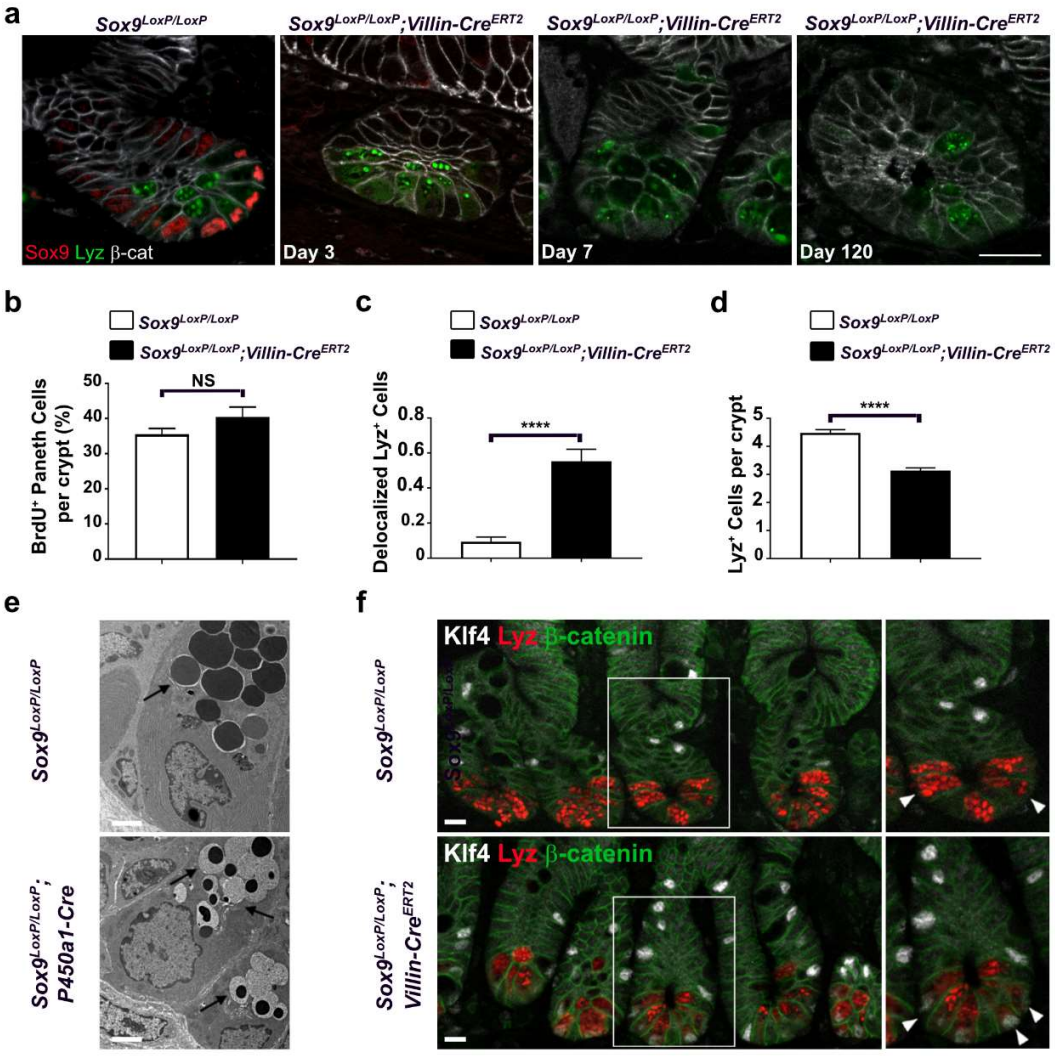

Fig S1

Figure S1 (related to Figure 1)

Sox9 deletion in adult epithelial cells triggers Paneth cell alterations.

a, Time course of Sox9 loss, 3 days, 7 days and 4 months after tamoxifen treatment. Sox9, Lyz and β-catenin co-stainings were obtained from *n* = 3 *Sox9*$^{LoxP/LoxP}$ mice, *n* = 2 *Sox9*$^{LoxP/LoxP}$*;Villin-Cre*^{ERT2} (3 days post-tamoxifen treatment), *n* = 3 *Sox9*$^{LoxP/LoxP}$*;Villin-Cre*^{ERT2} (7 days post-tamoxifen treatment) and *n* = 3 *Sox9*$^{LoxP/LoxP}$*;Villin-Cre*^{ERT2} (120 days post-tamoxifen treatment).

b, Quantification of BrdU^{+} Paneth cells 3 weeks after BrdU administration in drinking water in *Sox9*$^{LoxP/LoxP}$ and *Sox9*$^{LoxP/LoxP}$*;Villin-Cre*^{ERT2} mice. BrdU^{+} Paneth cells were quantified after

immunofluorescence staining for Lyz, BrdU and β-catenin. *n* = 50 crypt units per mouse; *n* = 3 *Sox9*$^{LoxP/LoxP}$*; Villin-Cre*^{ERT2} mice and *n* = 3 *Sox9*$^{LoxP/LoxP}$ mice.

c and d, Quantification of delocalized Paneth cells per crypt and Paneth cells per crypt in *Sox9*$^{LoxP/LoxP}$ and *Sox9*$^{LoxP/LoxP}$*;Villin-Cre*^{ERT2} mice. Staining for Lyz was performed on intestine sections from *n* = 3 *Sox9*$^{LoxP/LoxP}$*;Villin-Cre*^{ERT2} mice and *n* = 3 *Sox9*$^{LoxP/LoxP}$ mice, *n* = 50 crypt units per mouse were evaluated. Mice were sacrificed 2 weeks after tamoxifen treatment.

e, Electron micrographs from small intestine highlighting physiological secretory granules in Paneth cells (arrows) in control *Sox9*$^{LoxP/LoxP}$ *mice* whereas secretory granules in mice with a *Sox9* deletion in all epithelial cells except for Paneth cells (*Sox9*$^{LoxP/LoxP}$*;P450a1-Cre*; *n* = 2, 30 days post-BNF treatment) are abnormal one month after *Sox9* loss due to Paneth cell life span and their replacement by new, altered, Paneth cells.

f, Representative immunofluorescence co-staining of Lyz, β-catenin and Klf4, a transcription factor necessary for goblet cell differentiation, illustrating that Klf4 is absent in Paneth cells from control mice while it is expressed in Paneth cells when *Sox9* is deleted in epithelial cells (arrowhead). Paneth cell differentiation alterations were observed in *Sox9*$^{LoxP/LoxP}$*;Villin-Cre*^{ERT2} mice soon after *Sox9* deletion (1-4 days after tamoxifen treatment, *n* = 4 mice and *n* = 2 *Sox9*$^{LoxP/LoxP}$ mice) and were stable (7-50 days post-tamoxifen treatment, *n* = 6 *Sox9*$^{LoxP/LoxP}$*;Villin-Cre*^{ERT2} mice and *n* = 3 *Sox9*$^{LoxP/LoxP}$ mice).

Scale bars: 20 μm (**a**), 2 μm (**e**), 10 μm (**f**).

(b) and **(d)**, Mann-Whitney U test; NS: Not Significant; **** *P*<0.0001. **(b, c, d)** Data are shown as means ± S.E.M.

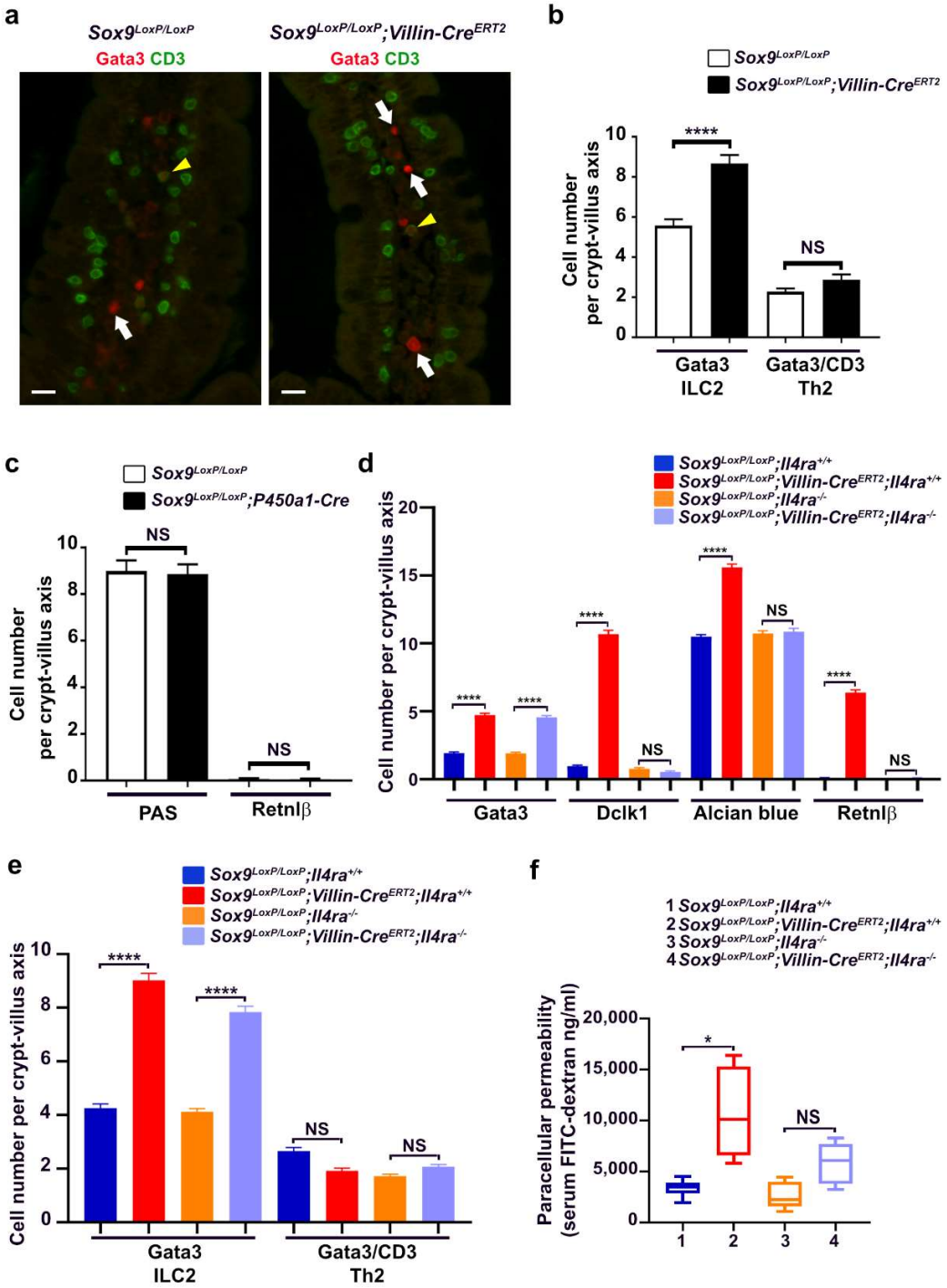
a
Sox9LoxP/LoxP
Gata3 CD3
Sox9LoxP/LoxP;Villin-CreERT2
Gata3 CD3
b
Sox9LoxP/LoxP
Sox9LoxP/LoxP;Villin-CreERT2
Cell number per crypt-villus axis
****
NS
Gata3 ILC2
Gata3/CD3 Th2
c
Sox9LoxP/LoxP
Sox9LoxP/LoxP;P450a1-Cre
Cell number per crypt-villus axis
NS
NS
PAS
RetnlB
d
Sox9LoxP/LoxP;Il4ra+/+
Sox9LoxP/LoxP;Villin-CreERT2;Il4ra+/+
Sox9LoxP/LoxP;Il4ra-/-
Sox9LoxP/LoxP;Villin-CreERT2;Il4ra-/-
Cell number per crypt-villus axis
Gata3
Dclk1
Alcian blue
RetnlB
e
Sox9LoxP/LoxP;Il4ra+/+
Sox9LoxP/LoxP;Villin-CreERT2;Il4ra+/+
Sox9LoxP/LoxP;Il4ra-/-
Sox9LoxP/LoxP;Villin-CreERT2;Il4ra-/-
Cell number per crypt-villus axis
Gata3 ILC2
Gata3/CD3 Th2
f
1 Sox9LoxP/LoxP;Il4ra+/+
2 Sox9LoxP/LoxP;Villin-CreERT2;Il4ra+/+
3 Sox9LoxP/LoxP;Il4ra-/-
4 Sox9LoxP/LoxP;Villin-CreERT2;Il4ra-/-
Paracellular permeability (serum FITC-dextran ng/ml)

Fig S2

Figure S2 (Related to Figure 3)

Active ILC2/IL13 signalling is required for epithelial remodelling in mice with abnormal Paneth cells

a, Representative immunofluorescence co-staining of Gata3 and CD3 in intestinal tissue from *Sox9$^{LoxP/LoxP}$* and *Sox9$^{LoxP/LoxP}$;Villin-Cre^{ERT2}* mice. Gata3^{+} cells correspond to ILC2 (white arrows) and Gata3^{+}/CD3^{+} cells are Th2 cells (yellow arrowheads). *n* = 3 mice per genotype were used. Mice were sacrificed 2 weeks after tamoxifen treatment.

b, Gata3^{+}/CD3^{-} and Gata3^{+}/CD3^{+} cells were counted in *n* = 50 crypt-villus units per mouse (*n* = 3 mice per genotype).

c, Quantification of PAS^{+} cells and Retnlβ^{+} cells in *Sox9$^{LoxP/LoxP}$;P450a1-Cre* mice. A type 2 immune response is absent when Paneth cells remain intact. Cells were counted in *n* = 50 crypt-villus units per mouse (*n* = 3 mice per genotype, sacrificed 10 days after BNF treatment).

d, Quantification of type 2 immune response markers in *Sox9$^{LoxP/LoxP}$* and *Sox9$^{LoxP/LoxP}$;Villin-Cre^{ERT2}* mice and in *Sox9$^{LoxP/LoxP}$;Villin-Cre^{ERT2};Il4ra$^{-/-}$* mice. Cells positive for Dclk1, PAS, Retnlβ, Gata3 or Alcian blue were counted in *n* = 50 crypt-villus units per mouse (*n* = 3 mice per genotype). Mice were sacrificed 2 weeks after tamoxifen treatment.

e, Quantification of Gata3^{+}/CD3^{-} and Gata3^{+}/CD3^{+} cells in *Sox9$^{LoxP/LoxP}$;Villin-Cre^{ERT2};Il4ra$^{-/-}$* mice. Positive cells were counted in *n* = 50 crypt-villus units per mouse (*n* = 3 mice per genotype). Mice were sacrificed 2 weeks after tamoxifen treatment.

f, Intestinal permeability, assessed by oral gavage of FITC-dextran, remains intact when Sox9 is deleted in an *Il-4Rα*–deficient mouse model. FITC-dextran was measured in serum from *Sox9$^{LoxP/LoxP}$;Il-4Ra$^{+/+}$* mice (*n*=6), *Sox9$^{LoxP/LoxP}$;Villin-Cre^{ERT2};Il-4Ra$^{+/+}$* mice (*n* = 5), *Sox9$^{LoxP/LoxP}$;Il-4Ra$^{-/-}$* mice (*n* = 7) and *Sox9$^{LoxP/LoxP}$;Villin-Cre^{ERT2};Il-4Ra$^{-/-}$* mice (*n* = 6). Mice were sacrificed 2 weeks after tamoxifen treatment.

(**a**) Scale bars: 20 μm.

(**b**, **c**) Mann-Whitney U test or Kruskal-Wallis test with Dunn's post hoc test (**d, e and f**); NS: Not Significant; **P*<0.05; **** *P*<0.0001. **(b, c, d and e)** Data are shown as means ± S.E.M.**(f)** The line indicates the median, the box marks the 25th and 75th percentiles and the whiskers indicate the minimal to maximum values.

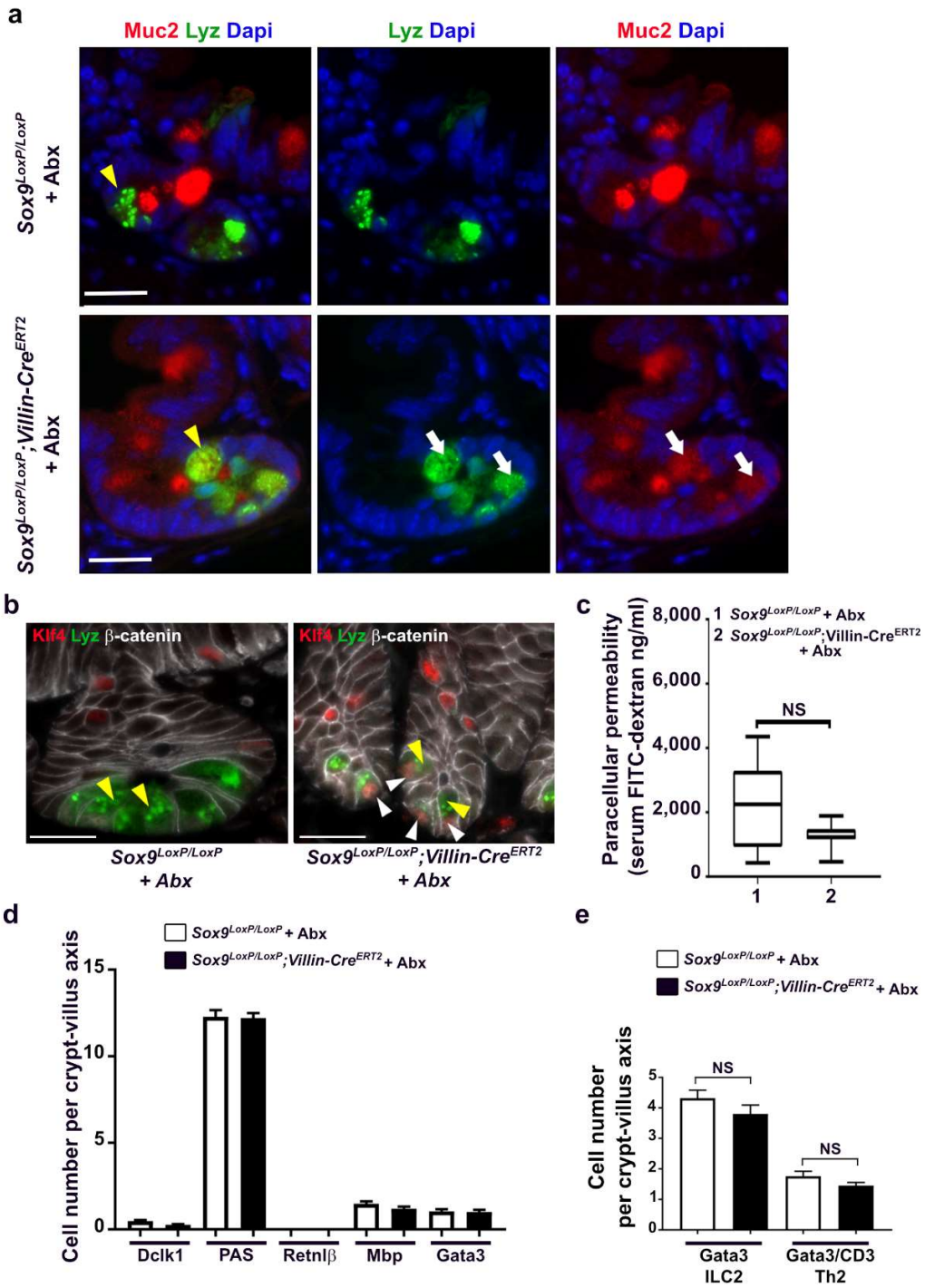

Fig. S3

Figure S3 (related to Figure 3)

Presence of a microbiota is required for intestinal permeability defaults and remodelled mucosal immunity in mice with altered Paneth cells

a, Representative immunofluorescence co-staining of Muc2 and Lyz show that Paneth cell differentiation defaults are maintained in mice receiving antibiotherapy (Abx). Muc2 is expressed in Paneth cells in *Sox9$^{LoxP/LoxP}$;Villin-Cre^{ERT2}* mice treated with Abx (white arrows), while it is absent in Paneth cells in *Sox9$^{LoxP/LoxP}$* mice. Lyz staining is diffuse in Sox9-deficient mice receiving Abx while it is bright and intense in control mice (yellow arrowheads). *n* = 3 mice per genotype. Abx = antibiotics. Mice were treated with tamoxifen and Abx for 5 days and then with Abx only for 2 more weeks.

b, Representative immunofluorescence co-staining of Klf4, Lyz and β-catenin show that alterations in Paneth cell identity are maintained in *Sox9$^{LoxP/LoxP}$;Villin-Cre^{ERT2}* mice treated with antibiotics (Abx). Klf4 is expressed in Paneth cells in *Sox9$^{LoxP/LoxP}$;Villin-Cre^{ERT2}* treated with a cocktail of antibiotics but not in *Sox9$^{LoxP/LoxP}$* mice (white arrowheads), and Lyz staining is diffuse in Sox9-deficient Paneth cells (yellow arrowheads). Abx = antibiotics. *n* = 3 mice per genotype. Mice were treated with tamoxifen and Abx for 5 days and then with Abx only for 2 more weeks.

c, Antibiotic treatment restores an intact intestinal barrier function. FITC-dextran dosage in serum is similar in antibiotics-treated *Sox9$^{LoxP/LoxP}$* (*n* = 8) and *Sox9$^{LoxP/LoxP}$;Villin-Cre^{ERT2}* mice (*n* = 7).

d, Type 2 immune response is abolished by antibiotics treatment. Cells positive for Dclk1, PAS, Retnlβ, Mbp or Gata3 were counted in *n* = 50 crypt-villus units per mouse (*n* = 3 mice per genotype).

e, Dysbiosis is required to induce a type 2 immune response. Quantification of ILC2 and Th2 cells (Gata3^{+}/CD3^{-} cells and Gata3^{+}/CD3^{+} cells, respectively) show that cell numbers are similar in *Sox9$^{LoxP/LoxP}$* and *Sox9$^{LoxP/LoxP}$;Villin-Cre^{ERT2}* mice treated with Abx. Immunofluorescence co-staining for Gata3 and CD3 was performed in intestinal tissue from *n* = 3 mice per genotype. Cells were counted in *n* = 50 crypt-villus units per mouse.

Scale bars: 20 μm (**a and b**).

(**c,d and e**) Mann-Whitney U test; NS: Not Significant. **(c)** The line indicates the median, the box marks the 25th and 75th percentiles and the whiskers indicate the minimal to maximum values. **(d and e)** Data are shown as means ± S.E.M.

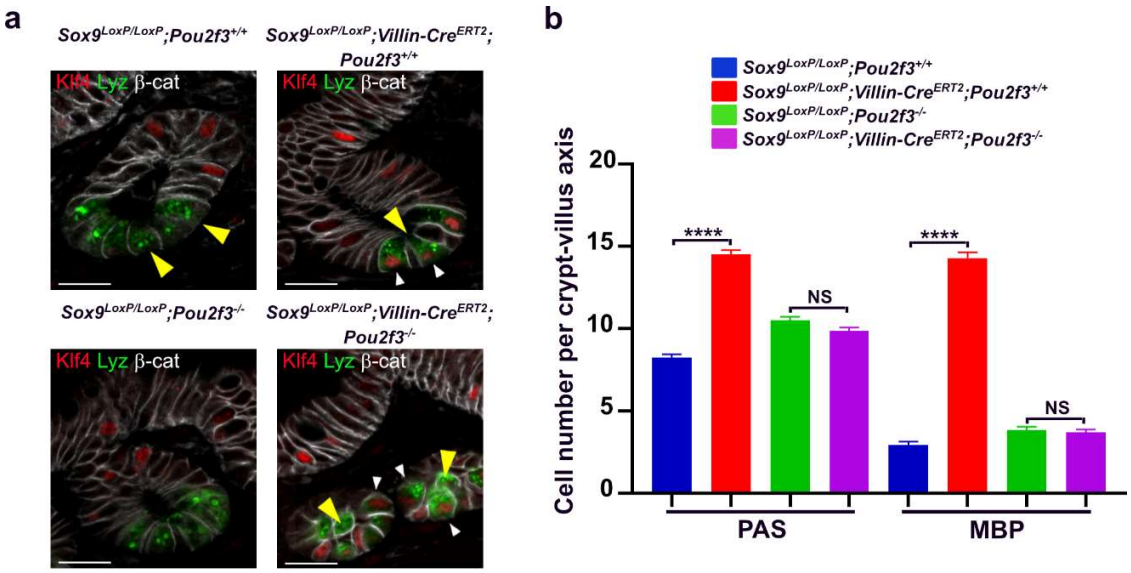

Fig. S4.

Figure S4 (related to Figure 4)

Tuft cells are essential for type 2 immune response development consecutive to Paneth cell dysfunction.

a, Representative immunofluorescence co-staining of Klf4, Lyz and β-catenin in *Sox9$^{LoxP/LoxP}$;Villin-Cre^{ERT2};Pou2f3$^{-/-}$* mice. Sox9-deleted Paneth cells display an ectopic expression of Klf4 in presence or absence of tuft cells (white arrowhead), and Lyz staining is diffuse in both genotypes compared to control mice (yellow arrowhead). *n* = 3 mice per genotype. Mice were sacrificed 2 weeks after tamoxifen treatment.

b, Quantification of PAS and MBP-positive cells in *Sox9$^{LoxP/LoxP}$;Villin-Cre^{ERT2};Pou2f3$^{-/-}$* mice. Cells were counted in *n* = 50 crypt-villus units per mouse (*n* = 3 *Sox9$^{LoxP/LoxP}$;Pou2f3$^{+/+}$* mice, *n* = 8 *Sox9$^{LoxP/LoxP}$;Villin-Cre^{ERT2};Pou2f3$^{+/+}$* mice, *n* = 6 *Sox9$^{LoxP/LoxP}$;Pou2f3$^{-/-}$* mice, *n* = 8 *Sox9$^{LoxP/LoxP}$;Villin-Cre^{ERT2};Pou2f3$^{-/-}$* mice). Mice were sacrificed 2 weeks after tamoxifen treatment. Scale bars: 20 μm (**a**). (**b**) Kruskal-Wallis test with Dunn's post hoc test; NS: Not Significant; ****P<0.0001. **(b)** Data are shown as means ± S.E.M.

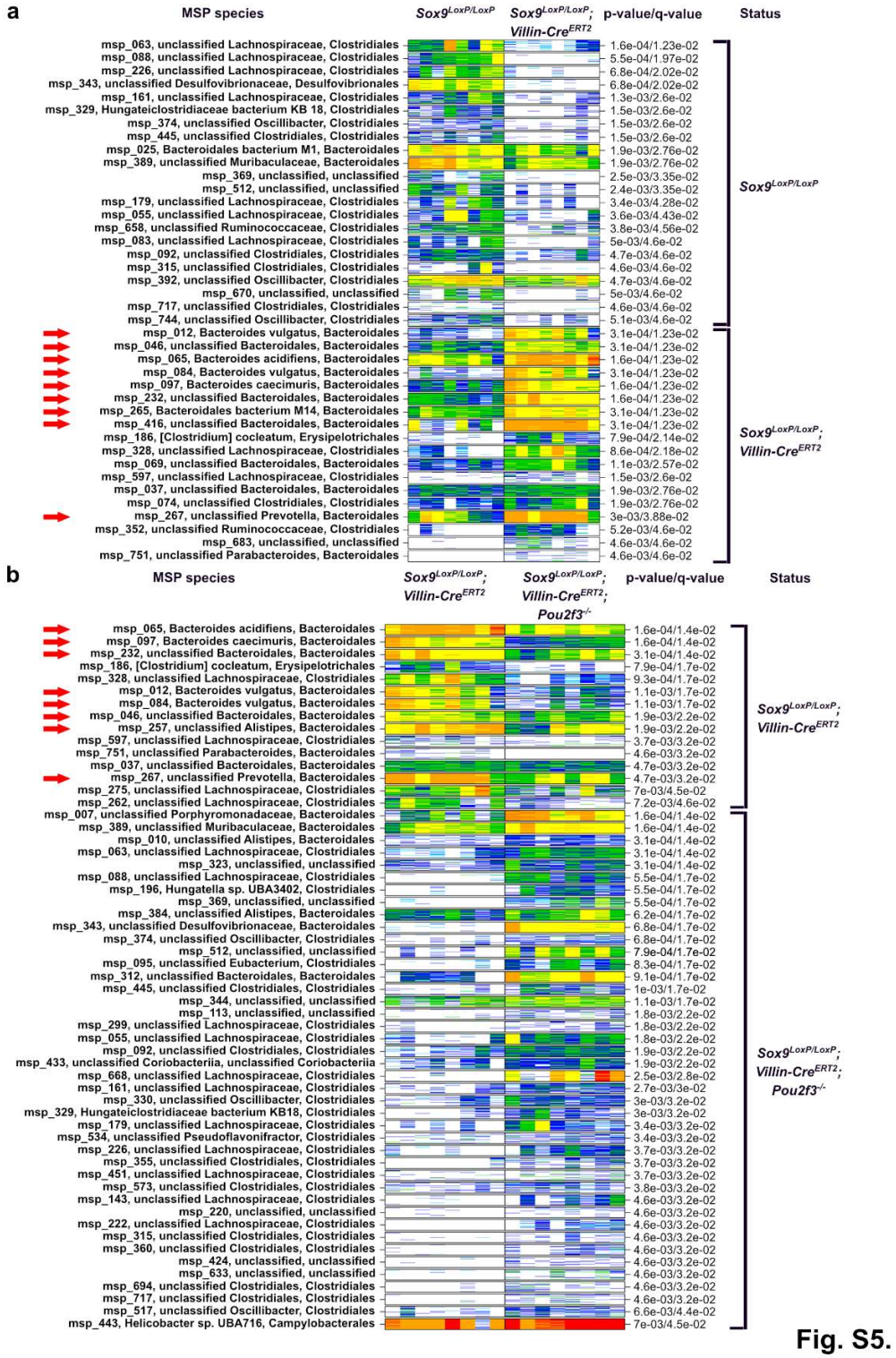

Fig. S5.

Figure S5 (related to Figure 5)

Tuft cell-induced type 2 immunity consecutive to Paneth cell defaults causes major alterations in microbiota composition.

a, Plot-Barcode of 40 differentially represented MSP species in caecum from *Sox9*$^{LoxP/LoxP}$ and *Sox9*$^{LoxP/LoxP}$*;Villin-Cre*^{ERT2} mice (q-value ≤ 0.05).

b, Plot-Barcode of 57 top differentially abundant MSP species in caecum from *Sox9*$^{LoxP/LoxP}$*;Villin-Cre*^{ERT2} and *Sox9*$^{LoxP/LoxP}$*;Villin-Cre*^{ERT2};*Pou2f3*$^{-/-}$ mice. MSP species of the *Bacteroidales* order were enriched in *Sox9*$^{LoxP/LoxP}$*;Villin-Cre*^{ERT2} mice as compared to control and *Sox9*$^{LoxP/LoxP}$*;Villin-Cre*^{ERT2};*Pou2f3*$^{-/-}$ mice (red arrows).

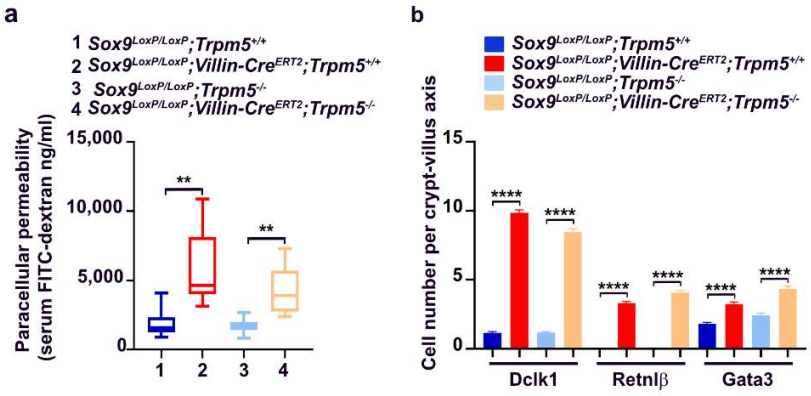

Fig S6

Figure S6 (related to Figure 5)

Induction of tuft cell-induced type 2 immunity in the context of defective Paneth cells is independent of Trpm5.

a, Intestinal permeability, assessed by FITC-dextran gavage, is altered when Sox9 is deleted in a Trpm5 deficient context. FITC-dextran was measured in serum from *Sox9$^{LoxP/LoxP}$;Trpm5$^{+/+}$* mice (*n* = 9), *Sox9$^{LoxP/LoxP}$;Villin-Cre^{ERT2} ;Trpm5$^{+/+}$*mice (*n* = 8), *Sox9$^{LoxP/LoxP}$;Trpm5$^{-/-}$* mice (*n* = 11) and *Sox9$^{LoxP/LoxP}$;Villin-Cre^{ERT2};*Trpm5$^{-/-}$ mice (*n* = 12). Mice were sacrificed 2 weeks after tamoxifen treatment.

b, Type 2 immune response is present in the absence of Trpm5. Cells positive for Dclk1, Retnlβ, or Gata3 were counted in *n* = 50 crypt-villus units per mouse (*n* = 3 mice per genotype).

(a,b) Kruskal-Wallis test with Dunn's post hoc test; NS: Not Significant; ***P*<0.01; *****P*<0.0001. **(a)** The line indicates the median, the box marks the 25th and 75th percentiles and the whiskers indicate the minimal to maximum values. **(b)** Data are shown as means ± S.E.M.

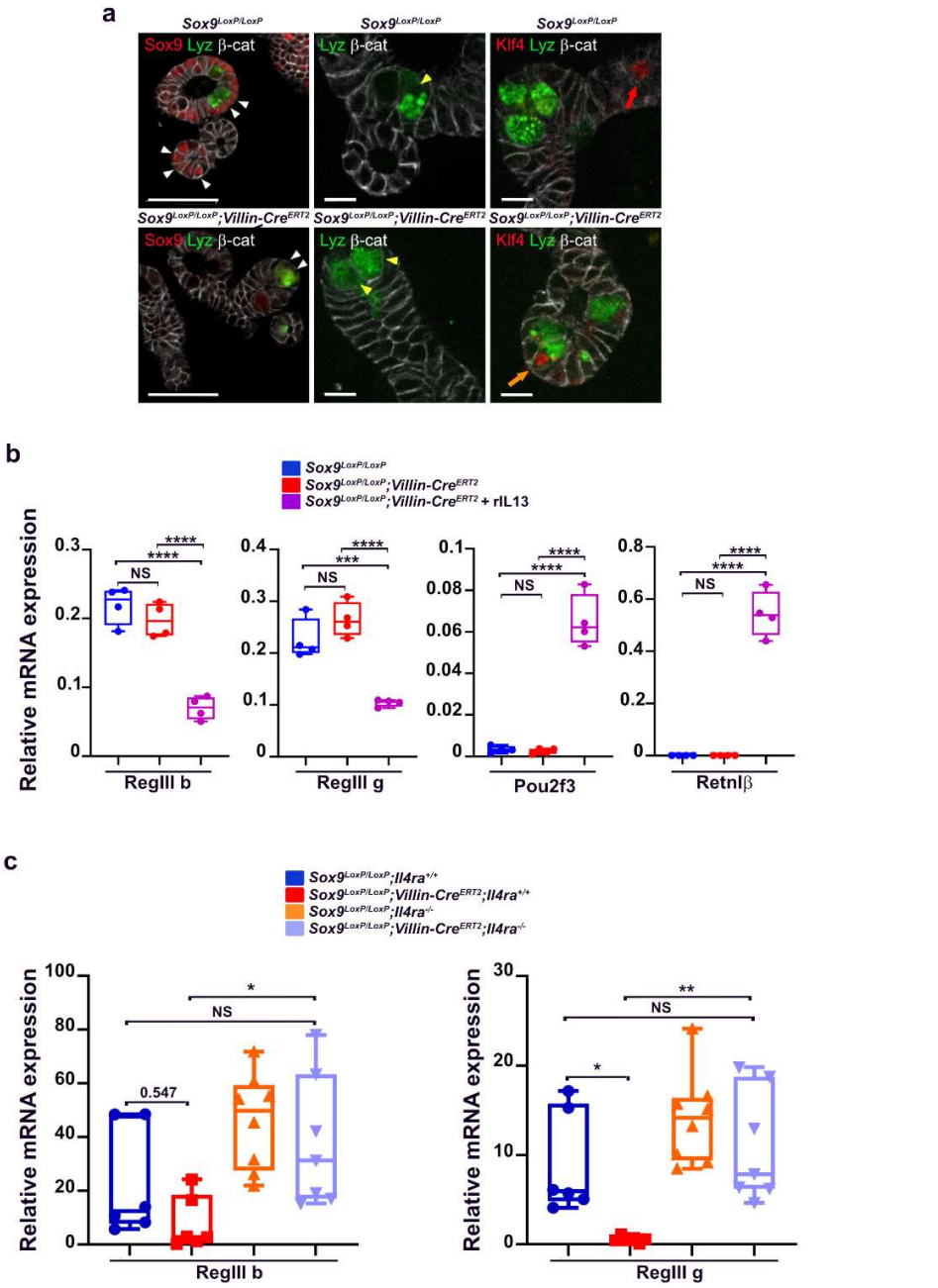

Fig. S7

Figure S7 (related to Figure 6)

Type 2 cytokines amplify initial Paneth cell defects via down-regulation of the antimicrobial peptide RegIII

a, Representative immunofluorescence co-staining of Sox9, Lyz and β-catenin, and Klf4, Lyz and β-catenin in organoids derived from *Sox9$^{LoxP/LoxP}$;Villin-Cre^{ERT2}* mice. Sox9 was not detected 5 days after 4-OH-tamoxifen treatment in *Sox9$^{LoxP/LoxP}$;Villin-Cre^{ERT2}* organoids (white arrow-heads, scale bars, 50 μm). Lyz staining was diffuse in *Sox9$^{LoxP/LoxP}$;Villin-Cre^{ERT2}* organoids (yellow arrow-heads, scale bars, 20 μm), and ectopic expression of Klf4 was present in Paneth cells when Sox9 was deleted (orange arrow, scale bars, 20 μm), but was express in mucus-secreting cells in control organoids (red arrow, scale bars, 20 μm). Organoids were treated for 3 days with 4-OH-tamoxifen and analysed 5 days after treatment. Experiments from 2 independent organoid cultures, repeated 3 times.

b, RT-qPCR analysis of antimicrobial peptides *RegIIIβ and RegIIIγ, Pou2f3* and *Retnlβ* genes in organoids derived from *Sox9$^{LoxP/LoxP}$* and *Sox9$^{LoxP/LoxP}$;Villin-Cre^{ERT2}* small intestine, in the absence or presence of rIL-13 treatment. Organoids were treated with 4-OH-tamoxifen for 3 days and then incubated with rIL-13 (100 ng/ml) for 72 h. Triplicate experiments from 2 independent organoid cultures.

c, RT-qPCR analysis of antimicrobial peptides *RegIIIβ and RegIIIγ* in *Sox9$^{LoxP/LoxP}$*, *Sox9$^{LoxP/LoxP}$;Villin-Cre^{ERT2}* mice and in *Sox9$^{LoxP/LoxP}$;Villin-Cre^{ERT2};Il4ra$^{-/-}$* mice. (*n* = 6-8 mice per genotype). Mice were sacrificed 2 weeks after tamoxifen treatment.

(b, c) Kruskal-Wallis test with Dunn's post hoc test; NS: Not Significant; **P*<0.05; ***P*<0.01; ****P*<0.001; *****P*<0.0001. **(a, b)** The line indicates the median, the box marks the 25th and 75th percentiles and the whiskers indicate the minimal to maximum values.

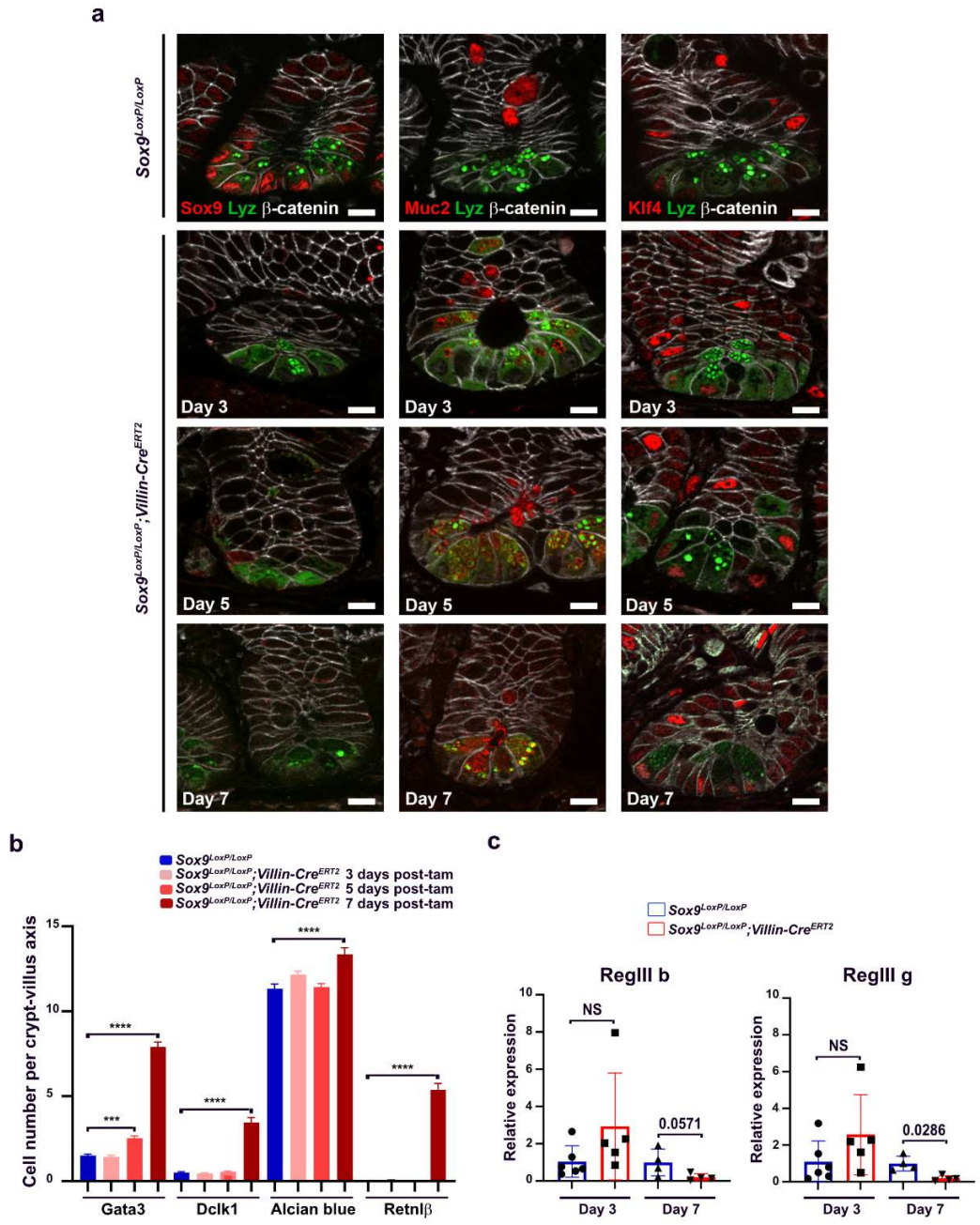

Fig S8

Figure S8 (related to Figure 7)

Kinetics of cellular and molecular events occurring in epithelial and *lamina propria* immune cells following alteration of Paneth cell function.

a, Representative immunofluorescence co-staining of Sox9, Lyz and β-catenin, Muc2, Lyz and β-catenin, and Klf4, Lyz and β-catenin in *Sox9$^{LoxP/LoxP}$;Villin-Cre^{ERT2}* mice at 3, 5 and 7 days following tamoxifen administration. Sox9 was not detected by 3 days after tamoxifen treatment in

Sox9$^{LoxP/LoxP}$*;Villin-Cre*^{ERT2} mice. Lyz staining was diffuse in *Sox9*$^{LoxP/LoxP}$*;Villin-Cre*^{ERT2} mice as early as 3 days after tamoxifen treatment. In addition, ectopic expression of Muc2 and Klf4 was present in Paneth cells 3 days after Sox9 deletion. *n* = 4-6 mice per condition.

b, Gata3^{+} cell numbers were increased by 3 days after tamoxifen treatment, while epithelial remodelling (characterized by an increased tuft cell and Goblet cell number and an ectopic expression of Retnlβ in Goblet cells) was present 5 days after tamoxifen treatment. Cells positive for Gata3, Dclk1, Alcian blue or Retnlβ were counted in *n* = 50 crypt-villus units per mouse (*n* = 4-6 mice per condition).

c, RT-qPCR analysis of antimicrobial peptides *RegIIIβ and RegIIIγ* in *Sox9*$^{LoxP/LoxP}$ and *Sox9*$^{LoxP/LoxP}$*;Villin-Cre*^{ERT2} mice at 3 and 7 days after tamoxifen treatment (*n* = 4-6 mice per condition).

(a) Scale bars, 10 μm.

(b) Kruskal-Wallis test with Dunn's post hoc test; (c) Mann-Whitney U test; NS: Not Significant; ***P<0.001; ****P<0.0001.

(a) Data are shown as means ± S.E.M. **(b)** The line indicates the median, the box marks the 25th and 75th percentiles and the whiskers indicate the minimal to maximum values.

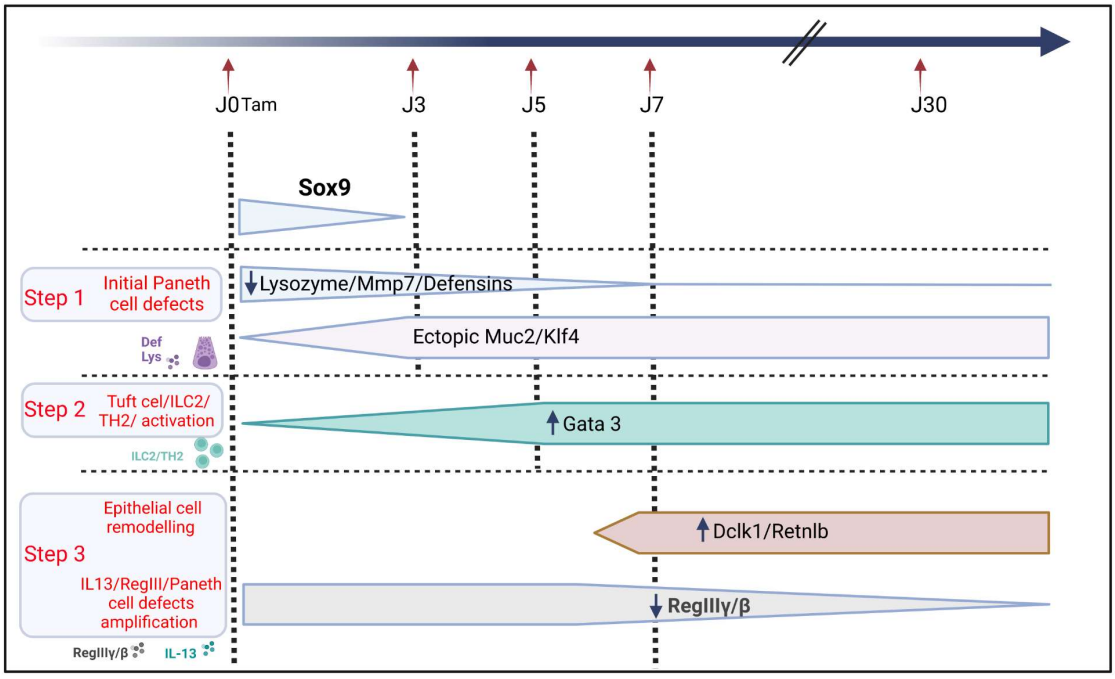

Figure S9 (related to Figure 7)

Schematic view of the sequence of cellular and molecular events occurring in epithelial and *lamina propria* immune cells following alteration of Paneth cell function induced by *Sox9* deletion, underlying the step-wise establishment of dysbiosis.

Table S1: Enrichment of gut metabolic modules (GMM) in the caecum of mice with wildtype versus *Sox9*-deficient Paneth cells

GMM_module	*p*-value	*q*-value	Enriched genotype	Module_definition	Primary_module_metabolism_definition	Second_module_metabolism_definition
MF0049	0.0001554	0.0024864	$Sox9^{Loxp/LoxP}$;$VillinCre^{ERT2}$	maltose degradation	carbohydrate degradation	disaccharide degradation
MF0052	0.0001554	0.0024864	$Sox9^{Loxp/LoxP}$;$VillinCre^{ERT2}$	chondroitin sulfate and dermatan sulfate degradation	carbohydrate degradation	glycosaminoglycan degradation
MF0059	0.0001554	0.0024864	$Sox9^{Loxp/LoxP}$;$VillinCre^{ERT2}$	rhamnose degradation	carbohydrate degradation	monosaccharide degradation
MF0064	0.0001554	0.0024864	$Sox9^{Loxp/LoxP}$;$VillinCre^{ERT2}$	pectin degradation	carbohydrate degradation	polysaccharide degradation
MF0082	0.0001554	0.0024864	$Sox9^{Loxp/LoxP}$;$VillinCre^{ERT2}$	pentose phosphate pathway (oxidative branch)	central metabolism	energy metabolism
MF0092	0.0001554	0.0024864	$Sox9^{Loxp/LoxP}$;$VillinCre^{ERT2}$	kdo2-lipid A synthesis	endotoxin biosynthesis	lipopolysaccharide biosynthesis
MF0101	0.0001554	0.0024864	$Sox9^{Loxp/LoxP}$;$VillinCre^{ERT2}$	Sulfate reduction (assimilatory)	gas metabolism	sulfate metabolism
MF0133	0.0001554	0.0024864	$Sox9^{Loxp/LoxP}$;$VillinCre^{ERT2}$	menaquinone production	secondary metabolites	vitamins
MF0018	0.0003108	0.00361659	$Sox9^{Loxp/LoxP}$;$VillinCre^{ERT2}$	proline degradation (glutamate pathway)	amino acid degradation	nonpolar. aliphatic amino acid degradation
MF0048	0.0003108	0.00361659	$Sox9^{Loxp/LoxP}$;$VillinCre^{ERT2}$	lactose degradation	carbohydrate degradation	disaccharide degradation
MF0065	0.0003108	0.00361659	$Sox9^{Loxp/LoxP}$;$VillinCre^{ERT2}$	pectin degradation - 5-dehydro-4-deoxy-D-glucuronate degradation	carbohydrate degradation	polysaccharide degradation
MF0025	0.0006216	0.0049728	$Sox9^{Loxp/LoxP}$;$VillinCre^{ERT2}$	alanine degradation (glutamate pathway)	amino acid degradation	nonpolar. aliphatic amino acid degradation
MF0041	0.0006216	0.0049728	$Sox9^{Loxp/LoxP}$;$VillinCre^{ERT2}$	histidine degradation	amino acid degradation	positively charged amino acid degradation
MF0053	0.0006216	0.0049728	$Sox9^{Loxp/LoxP}$;$VillinCre^{ERT2}$	allose degradation	carbohydrate degradation	monosaccharide degradation
MF0079	0.0006216	0.0049728	$Sox9^{Loxp/LoxP}$;$VillinCre^{ERT2}$	bifidobacterium shunt	central metabolism	energy metabolism
MF0127	0.0006216	0.0049728	$Sox9^{Loxp/LoxP}$;$VillinCre^{ERT2}$	Succinate production	organic acid metabolism	succinate metabolism
MF0100	0.00093097	0.00700967	$Sox9^{Loxp/LoxP}$	Sulfate reduction (dissimilatory)	gas metabolism	sulfate metabolism
MF0102	0.0010878	0.00773547	$Sox9^{Loxp/LoxP}$;$VillinCre^{ERT2}$	mucin degradation	glycoprotein degradation	mucus degradation

Table S2: list of the primers used

Gene name	Forward primer	Reverse primer
RegIIIg	CAGACAAGATGCTTCCCCGT	GCAACTTCACCTTGCACCTG
RegIIIb	TACTGCCTTAGACCGTGCTTTCTG	GACATAGGGCAACTTCACCTCACA
Lyz1	GAGACCGAAGCACCGACTATG	CGGTTTTGACATTGTGTTCGC
Mmp7	CGGTTTTGACATTGTGTTCGC	GGAAGTTCACTCCTGCGTCC
Defa29	CTCCTCTCTGCCCTCGTTCT	GAAACCTTCTTTGGGCTACATCTT
Tbx21	GTATCCTGTTCCCAGCCGTTTC	ACTGTGTTCCCGAGGTGTCC
Infg	CGGCACAGTCATTGAAAGCC	TGTCACCATCCTTTTGCCAGT
Tnfa	TAGCCCACGTCGTAGCAAAC	GCAGCCTTGTCCCTTGAAGA
Gata3	CTCGGCATTCGTACATGGAA	GGATACCTCTGCACCGTAGC
Il4	TGAGCTCGTCTGTAGGGCTT	GTGCAGCTTATCGATGAATCCAG
Il13	ACATCACACAAGACCAGACTCC	CTTGCGGTTACAGAGGCCAT
Il17	CTCCAGAAGGCCCTCAGACTAC	AGCTTTCCCTCCGCATTGACACAG
Il21	ATCCTGAACTTCTATCAGCTCCAC	GCATTTAGCTATGTGCTTCTGTTTC
Il22	GCTCAGCTCCTGTCACATCA	CAGTTCCCCAATCGCCTTGA
Il25	CCTGTCAGGCAGGGGTAGTA	CCAAGAATGCAACAGCCTGG
Il33	GCTGCGTCTGTTGACACATTGAG	GGTCTTGCTCTTGGTCTTTTCCAG
Rorc	CCGCTGAGAGGGCTTCAC	TGCAGGAGTAGGCCACATTACA
Pou2f3	GAGGGAATGATGAGCCCACT	GTGAAGCCTAGCTTAATGCGTC
Retnlb	ATGGTTGTCACTGGATGTGC	TGGCAGTGGCAAGTATTTCC

Materials and Methods

Animal procedures

Sox9$^{LoxP/LoxP}$*;Villin-Cre*^{ERT2} mice and their controls *Sox9*$^{LoxP/LoxP}$ mice received an antibiotic treatment administered by oral gavage (300 µl) at daily dose consisting of 5 mg.ml^{-1} vancomycin (Sigma-Aldrich), 0.1 mg.ml^{-1} amphotericin B (Sigma-Aldrich), 10 mg.ml^{-1} metronidazole (Sigma-Aldrich), 10 mg.ml^{-1} neomycin (Sigma-Aldrich). Ampicillin (Sigma-Aldrich) was given in drinking water (1 g.l^{-1}) and bottles were changed 2-3 times per week. Mice were treated with antibiotic cocktail and tamoxifen (1 mg) during 5 days and then with antibiotics only during 2 weeks.
5-Bromo-2'-deoxyuridine (5-BrdU, Sigma-Aldrich) was given to *Sox9*$^{LoxP/LoxP}$ and *Sox9*$^{LoxP/LoxP}$*;Villin-Cre*^{ERT2} mice in drinking water (0.1 g.l^{-1}) for 3 weeks.

RNA extraction and qPCR

Total RNA was extracted from snap-frozen intestinal tissues using TRIzol reagent (Life Technologies) and then precipitated with isopropanol. RNA was further purified on RNeasy columns (Qiagen) and treated with DNAse (Qiagen). RNA was quantified with NanoDrop Spectrophotometer (Thermo Scientific). First strand cDNA synthesis was performed with 1 µg purified RNA using Transcriptor First Strand cDNA synthesis KIT (Roche Diagnostics) according to the manufacturer's instructions. Gene expression was quantified by qRT-PCR experiments using LightCycler 480 SYBR Green I Master (Roche Diagnostics) and were performed on LightCycler 480 system. Primer sets used for each gene analysed are presented in Table S2. Data were normalized to the expression levels of *GAPDH*, *Hprt* and *Mrpl32*. Stability of the references genes was evaluated using *geNorm* (1) and relative expression were determined using the threshold cycle relative quantification method.

Transmission electron microscopy

Small biopsies of intestinal tissues were fixed with 2.5% glutaraldehyde for 2-3 hours at RT and then O/N at 4°C. Biopsies were post-fixed with 0.5% osmium tetroxide and 0.8% potassium ferricyanide, dehydrated with a graded ethanol and acetone, and finally embedded in epoxy resin. Tissue sections were embedded in EmBed 812 using an Automated Microwave Tissue Processor for Electronic Microscopy, Leica EM AMW. Thin sections (70 nm; Leica-Reichert Ultracut E) were collected at different levels of each block. These sections were counterstained with uranyl acetate 1.5% in 70% Ethanol and lead citrate. Sections were visualized using a transmission electron microscope Hitachi 7100 equipped with a digital ORCA-SR camera (Hamamatsu) or using a Tecnai

F20 transmission electron microscope at 200KV in the CoMET MRI facilities, Institut des Neurosciences de Montpellier, Biocampus Montpellier France.

Intestinal permeability measurement using FITC-dextran

Mice were starved for 4 hours, received FITC-dextran by oral gavage (600 mg per kg of body weight), and blood was collected by cardiac puncture 4 hours after FITC-dextran administration. Blood was centrifuged at 3000 rpm for 20 minutes at 4°C and serum was collected. Fluorescence intensity contained in serum was measured using INFINITE F500 (Tecan) and serum FITC concentration was quantified using a standard curve.

Fluorescent and bright-field immunohistochemistry on paraffin-embedded tissue

Intestinal tissues were fixed in neutral-buffered formalin for 24 hours at RT, embedded in paraffin and tissue sections (4 μm) were prepared with a microtome (MICROM). Sections were incubated in successive baths of xylene and ethanol and antigen retrieval was performed by boiling the sections with 10 mM sodium citrate (pH 6.4) for 20 minutes. Primary antibodies used to stain the sections were : anti-Sox9 (HPA001758, Sigma-Aldrich), anti-Lysozyme C (C-19, Santa Cruz Biotechnology), anti-βcatenin (610154, BD Biosciences), anti-Klf4 (HPA 002926, Sigma-Aldrich), anti-Mucin2 (Sc15334, Santa Cruz Biotechnology), anti-BrdU (G3G4, Hybridoma Bank), anti-Gata3 (ab199428, Abcam), anti-Dclk1 (ab31704, Abcam), anti-Retlnβ (ABIN465494, Antibodies online), anti-MBP (Mayo Clinic), and anti-CD3 (ab11089, Abcam). For fluorescent immunochemistry, sections were incubated with fluorescent secondary antibodies conjugated with Alexa-488, cyanin3 or cyanin5 (Jackson ImmunoResearch Laboratories, Inc.) and Hoechst (2 μg/ml, Sigma-Aldrich). For bright-field immunochemistry experiments, N-Histofine (Nicheiri Biosciences Inc.) was used as secondary reagent, stainings were revealed using DAB (Sigma-Aldrich), and sections were counterstained with haematoxylin (Sigma-Aldrich).

Microscopy and imaging

Fluorescent images were acquired with an AxioImager Z1 microscope (Carl Zeiss, Inc.) equipped with an AxioCam MRm camera (Carl Zeiss, Inc.), the Apotome Slider system (Carl Zeiss, Inc.) and Zen software (Carl Zeiss, Inc.). Bright-field immunochemistry images were acquired with an Eclipse 80i microscope (Nikon) equipped with a digital camera (Q-imaging Retiga 2000R), and Q-Capture Pro software (Nikon). Treatment of images and panel composition were performed using Photoshop software (Adobe).

Fecal bacterial DNA isolation and 16S rRNA sequencing

Microbial communities profiling was performed by GenoScreen (Lille, France). Faeces were collected from *Sox9*$^{LoxP/LoxP}$ and *Sox9*$^{LoxP/LoxP}$*;Villin-Cre*^{ERT2} mice (n = 8 per genotype) 30 days after tamoxifen treatment and rapidly snap frozen. gDNA was extracted using a GenoScreen optimized protocol based on commercially available extraction kit (QIAamp Fast DNA Stool Mini Kit, Qiagen). 16S rDNA-amplicon library was prepared using a 16S primer pair that encompasses a 463 pb targeting the V3-V4 region, using a protocol developed by GenoScreen and named Metabiote®. The sequencing of the library was performed using MiSeq Illumina instrument with the V2 2*250pb chemistry. Taxonomic assignment has been developed and optimized by GenoScreen and is based on the use of the sofware QIIME 1.9.1. Microbial diversity and composition were generated using GenoScreen Bioinformatics package. Characterization of species diversity present within samples (alpha diversity) was calculated using the Shannon diversity index. The level of variation in species composition among samples (beta diversity) was quantified using weighted UniFrac (accounts for the relative abundance of each of the taxa within the communities) and unweighted-UniFrac distances. Statistical analyses of species abundance between samples were performed using 3 different tests: DeSeq2, Kruskal-Wallis and T-test.

Caecal DNA extraction and high throughput metagenomic sequencing

DNA extraction was performed following IHMS SOP 07 V2 for each sample. Briefly, samples underwent a thermal, chemical and mechanical lysis and operations to eliminate cell debris, proteins, aromatic compounds and RNA. Alcoholic precipitation of DNA salts was performed before cleaning and DNA pellet was reconstituted in TE buffer. Fluorometric Quantitation using Qubit (ThermoFisher Scientific) and FilterMax (Molecular devices) were used to assess the quantity of DNA and Fragment Analyzer 1.0 (Agilent Technologies) was used to assess DNA quality. 3 µg of high molecular weight DNA (>10 kbp) was sheared into fragments of approximately 150 bp using an ultrasonicator (Covaris, Woburn, US) and DNA fragment library construction was performed using the Ion Plus Fragment Library and Ion Xpress Barcode Adaptaters Kits (ThermoFisher Scientific, Waltham, US). Purified and amplified DNA fragment libraries were sequenced using the Ion Proton Sequencer (ThermoFisher Scientific, Waltham, US), with a minimum of 20 million high-quality reads generated per library.

Read Mapping Procedure

High throughput sequencing produced an average of 22.6 ± 1 million reads per sample, that were filtered of low quality reads (6 %; average) and host related reads (19%; average). Resulting high quality reads (average 17 ± 2.6 million) were mapped onto the BGI 2.6 million genes catalog (2) using our in-house METEOR software suite (https://forgemia.inra.fr/metagenopolis/meteor) (3).

Mapping was performed with an identity threshold of 95% to the reference gene catalog with Bowtie 2 (4) in a two steps procedure. First, unique mapped reads (reads mapped to a unique gene in the catalogue) were attributed to their corresponding genes and second, shared reads (reads that mapped with the same alignment score to multiple genes in the catalog) were weighted according to the ratio of unique mapping counts. Gene abundance table was rarefied, normalized and analyzed using MetaOMineR (momr) R package (https://github.com/eprifti/momr). Rarefaction was performed by randomly extracting 4 million reads per sample (to match the lowest mapped reads sample of 4.5 million reads) without replacement to avoid differences in sequencing depth and limit sample size artifacts on low abundant genes. Rarefied gene counts were normalized using the FPKM strategy (normalization by gene size and total number of mapped reads). Gene richness was calculated by counting the number of genes detected in the corresponding sample.

Metagenomic Species Pangenome (MSP) estimation

Metagenomic Species Pangenome (MSP) were used to quantify microbial species associated to the reference catalog. MSP are clusters of co-abundant genes (minimum cluster size ≥ 100 genes), used as proxy for microbial species, and reconstructed from the BGI 2.6 million genes catalogue into 811 MSP (5, 6). MSP abundance was calculated as the mean abundance of their 50 markers genes. A MSP detection limit was applied using a detection threshold of 10% of the marker genes. Taxonomical annotation was performed as described previously (6).

A total of 433 MSP species were detected across samples. MSP detected in at least 10% of the samples were kept for further analysis (362 MSP; 84%). Statistical analysis was performed under R version 3.4.2. Differences of MSP abundances between groups were determined using non parametric and unpaired Wilcoxon rank-sum tests and corrected for multiple tests using Benjamini-Hochberg procedure. Significant differences were considered using q-value ≤ 0.05. Differentially abundant MSP species were visualized using plotbarcodes and were organized in rows by blocks of their 50 marker genes and ranked by q-value and enrichment status. Within each block, barcoding plots (heatmaps) of the frequency abundances of the marker genes were represented (white, absent; light blue to red, low to high abundance). Mice were represented in columns by group and ordered by their MSP richness.

Assessment of the functional potential (GMM modules)

The metabolic potential of the mouse microbiome was assessed using an in-house pipeline. Genes of the BGI 2.6 million genes catalog (2) were annotated using Kyoto Encyclopedia of Genes and Genomes (KEGG) 82 database (7) using diamond tool (8) by considering the best-ranked KO among hits (e-value <10-5 and bit score > 60). Gut Metabolic Modules (GMM) (9) were reconstructed for each metagenomic MSP species using their pathway structures and potential

alternative pathways based on their detected annotated KO genes. Since MSP species are pangenomes (i.e. the collection of their 'core' and 'accessory' genes are known) (6), we considered a functional module to be present in a given species if at least 90% of its components were present in the 'core' genes of the corresponding MSP species. We then refined this calculation sample by sample, by adding the 'accessory' genes detected in a given sample. Abundance of each detected module in a MSP species corresponded to the abundance of the MSP itself. Abundance of a given module in a sample was computed as the sum of the modules' abundances of the detected metagenomic MSP species.

Quantitative analysis of succinate pathways components in mice gut microbiome

To address the potential of succinate production in the mice gut microbiome, we investigated enzymatic complexes of the reductive branch pathways of the TCA cycle, corresponding to the main succinate producing pathway used by anaerobic microorganisms (10). We focused on the two final steps, that is (1) the conversion of malate to fumarate by the fumarate hydratase (encoded by *fumABC*) and (2) the conversion of fumarate to succinate by the fumarate reductase (encoded by *frdABCD*). First, we collected all functional orthologs from the KO (KEGG Orthology) database described as *fumABC* or *frdABCD*. Two and three KO alternatives were found for *fumABC* and *frdABCD* enzymatic complexes, respectively (Figure 7A). Second, we annotated the 2.6 million genes from the BGI catalogue (2) with the KO database using diamond tool (8). Of note, all KOs from the *frdABCD* alternative coded as v3 (Figure 7A) were absent from the catalogue. Next, we computed the completeness of all *fumABC* and *frdABCD* alternatives in each MSP, based on the KO annotation of its gene content.

Completeness C of an alternative composed of KOs is defined here as the number of KOs detected in a given MSP and divided by the total number of KO in the alternative *n*.

$$C_{K1\cdots Kn} = \frac{\sum_{i=1}^{n} \mathrm{Presence(K}_i)}{\mathrm{n}}$$

$$\mathrm{Presence}(K_i) \in \{0,1\}\ (\forall\ i \in [1;n])$$

We assessed the global completeness of succinate production for a given MSP as the maximum completeness across all possible alternatives. Finally, we analyzed the global completeness of the differentially abundant MSP species enriched in *Sox9*$^{LoxP/LoxP}$ or *Sox9*$^{LoxP/LoxP}$*;Villin-Cre*^{ERT2} mice (FDR ≤ 0.05).

Organoid culture

Organoid lines were passaged twice and then cultured in a medium supplemented with 4-OH-tamoxifen (200 nM) resuspended in ethanol during 3 days to induce Sox9 deletion *in-vitro via* the Cre recombinase activation. Organoids were then collected 5 days after tamoxifen treatment. In some experiments, organoids were first treated with 4-OH-tamoxifen, and then incubated with rIL-13 (100 ng/ml) for 72h. Intestinal organoid RNA was isolated using the RNeasy Mini kit (Qiagen), or organoids were washed twice in cold PBS to dissolve the Matrigel, fixed overnight with 4% paraformaldehyde and included in Histogel (Thermo Scientific) before paraffin embedding.

References

1. J. Vandesompele, *et al.*, Accurate normalization of real-time quantitative RT-PCR data by geometric averaging of multiple internal control genes. *Genome Biol* **3**, research0034.1-research0034.11 (2002).

2. L. Xiao, *et al.*, A catalog of the mouse gut metagenome. *Nat Biotechnol* **33**, 1103–1108 (2015).

3. A. Cotillard, *et al.*, Dietary intervention impact on gut microbial gene richness. *Nature* **500**, 585–588 (2013).

4. B. Langmead, S. L. Salzberg, Fast gapped-read alignment with Bowtie 2. *Nature methods* **9**, 357 (2012).

5. H. B. Nielsen, *et al.*, Identification and assembly of genomes and genetic elements in complex metagenomic samples without using reference genomes. *Nat Biotechnol* **32**, 822–828 (2014).

6. F. Plaza Oñate, *et al.*, MSPminer: abundance-based reconstitution of microbial pan-genomes from shotgun metagenomic data. *Bioinformatics* **35**, 1544–1552 (2019).

7. M. Kanehisa, S. Goto, KEGG: Kyoto Encyclopedia of Genes and Genomes. 4 (2000).

8. B. Buchfink, C. Xie, D. H. Huson, Fast and sensitive protein alignment using DIAMOND. *Nat Methods* **12**, 59–60 (2015).

9. S. Vieira-Silva, *et al.*, Species–function relationships shape ecological properties of the human gut microbiome. *Nat Microbiol* **1**, 16088 (2016).

10. X. Liu, *et al.*, Biosynthetic Pathway and Metabolic Engineering of Succinic Acid. *Front. Bioeng. Biotechnol.* **10**, 843887 (2022).